OBSERVATIONS AND MODELLING OF THE INNER HELIOSPHERE

Propagation of Interplanetary Coronal Mass Ejections: The Drag-Based Model

**B. Vršnak · T. Žic · D. Vrbanec · M. Temmer ·
T. Rollett · C. Möstl · A. Veronig · J. Čalogović ·
M. Dumbović · S. Lulić · Y.-J. Moon · A. Shanmugaraju**

B. Vršnak (✉) · T. Žic · D. Vrbanec · J. Čalogović · M. Dumbović
Hvar Observatory, Faculty of Geodesy, University of Zagreb, Kačićeva 26, 10000 Zagreb, Croatia
e-mail: bvrsnak@geof.hr

T. Žic
e-mail: tzic@geof.hr

D. Vrbanec
e-mail: dijana.vrbanec@gmail.com

M. Temmer · T. Rollett · C. Möstl · A. Veronig
IGAM, Institute of Physics, University of Graz, Universitätsplatz 5, 8010 Graz, Austria

M. Temmer
e-mail: manuela.temmer@uni-graz.at

T. Rollett
e-mail: tanja.rollett@uni-graz.at

C. Möstl
e-mail: christian.moestl@uni-graz.at

A. Veronig
e-mail: astrid.veronig@uni-graz.at

C. Möstl
Space Science Laboratory, University of California, Berkeley, CA 94720, USA

S. Lulić
Karlovac University of Applied Sciences, Trg J.J.Strossmayera 9, 47000 Karlovac, Croatia
e-mail: slulic@vuka.hr

Y.-J. Moon
School of Space Research, Kyung Hee University, Yongin 446-701, Republic of Korea
e-mail: moonyj@khu.ac.kr

Abstract We present the "Drag-Based Model" (DBM) of heliospheric propagation of interplanetary coronal mass ejections (ICMEs). The DBM is based on the hypothesis that the driving Lorentz force, which launches a CME, ceases in the upper corona and that beyond a certain distance the dynamics becomes governed solely by the interaction of the ICME and the ambient solar wind. In particular, we consider the option where the drag acceleration has a quadratic dependence on the ICME relative speed, which is expected in a collisionless environment, where the drag is caused primarily by emission of magnetohydrodynamic (MHD) waves. In this paper we present the simplest version of DBM, where the equation of motion can be solved analytically, providing explicit solutions for the Sun–Earth ICME transit time and impact speed. This offers easy handling and straightforward application to real-time space-weather forecasting. Beside presenting the model itself, we perform an analysis of DBM performances, applying a statistical and case-study approach, which provides insight into the advantages and drawbacks of DBM. Finally, we present a public, DBM-based, online forecast tool.

1. Introduction

Prediction of the arrival of interplanetary coronal mass ejections (ICMEs) at 1 AU is one of the primary tasks of the space-weather forecasting, since ICMEs are responsible for major geomagnetic storms (*e.g.*, Koskinen and Huttunen, 2006). Thus, the research on heliospheric dynamics of ICMEs is essential in developing and advancing the forecast methods. The substantial progress in the observational aspect of the research achieved over the past decade is mainly related to the unprecedented observations gathered by the *Large Angle Spectroscopic Coronagraph* (LASCO; Brueckner *et al.*, 1995) onboard the *Solar and Heliospheric Observatory* (SoHO), the *Solar Mass Ejection Imager* (SMEI; Jackson *et al.*, 2004), and especially, the *Sun Earth Connection Coronal and Heliospheric Investigation* (SECCHI; Howard *et al.*, 2008) onboard the *Solar Terrestrial Relations Observatory* mission (STEREO-A and STEREO-B spacecraft). A significant contribution was provided also by meticulous analysis of radio-spectrographic measurements (*e.g.*, Reiner, Kaiser, and Bougeret, 2007, and references therein) and radio-scintillation measurements (*e.g.*, Manoharan, 2010, and references therein), as well as by *in-situ* solar-wind measurements from a number of space missions.

The advancement of observational techniques contributed to progress in various forms of modeling the heliospheric propagation of ICMEs, and maybe even more important, provided detailed testing of the related forecast procedures, either from the statistical point of view or in the form of case studies (for the validation of forecast methods see, *e.g.*, Cho *et al.*, 2003; Dryer *et al.*, 2004; Oler, 2004; Owens and Cargill, 2004; McKenna-Lawlor *et al.*, 2006, 2008; Tappin, 2006; Feng *et al.*, 2009; Smith *et al.*, 2009; Byrne *et al.*, 2010; Falkenberg *et al.*, 2010; Maloney and Gallagher, 2010; Taktakishvili *et al.*, 2009; Vršnak *et al.*, 2010; Falkenberg *et al.*, 2011 and references therein). The modeling and forecasting methods can be divided into several classes. On one side, there are purely empirical/statistical methods,

A. Shanmugaraju
Department of Physics, Arul Anandar College, Karumathur 625 514, Madurai, India
e-mail: ashanmugaraju@gmail.com

or kinematical-empirical methods, based on various relationships between the coronographically measured parameters and the ICME arrival time and/or characteristics of their heliospheric propagation (*e.g.*, Brueckner *et al.*, 1998; Gopalswamy *et al.*, 2000; Vršnak and Gopalswamy, 2002; Manoharan *et al.*, 2004; Michałek *et al.*, 2004; Schwenn *et al.*, 2005; Manoharan and Mujiber Rahman, 2011, and references therein). On the other side, there are numerical MHD-based models of the heliospheric propagation of ICMEs or shocks they are driving (*e.g.*, McKenna-Lawlor *et al.*, 2002; Fry *et al.*, 2003; González-Esparza *et al.*, 2003; Dryer *et al.*, 2004 Manchester *et al.*, 2004; Odstrcil, Riley, and Zhao, 2004; Odstrcil, Pizzo, and Arge, 2005; Smith *et al.*, 2009; Taktakishvili *et al.*, 2009, and references therein).

In between the empirical and numerical methods, there is a class of analytical, MHD- or HD-based, kinematical models of the ICME propagation. Most of them rely on the hypothesis that beyond a certain distance the ICME dynamics becomes governed solely by the interaction of the ICME and the ambient solar wind (Cargill, 2004; Owens and Cargill, 2004; Vršnak and Žic, 2007; Vršnak, Vrbanec, and Čalogović, 2008; Borgazzi *et al.*, 2009; Lara and Borgazzi, 2009; Vršnak *et al.*, 2010). This assumption is founded on the fact that in the interplanetary space fast ICMEs decelerate, whereas slow ones accelerate, showing a tendency to adjust their velocity to the ambient solar wind (*e.g.*, Gopalswamy *et al.*, 2001; Vršnak *et al.*, 2004; Yashiro *et al.*, 2004; Manoharan, 2006; Vršnak, Vrbanec, and Čalogović, 2008; Morrill *et al.*, 2009; Webb *et al.*, 2009).

In this paper we present a specific version of the drag-based model (hereafter DBM) that provides an analytical solution of the equation of motion, and we analyze its potentials for the real-time space-weather forecasting. The model is based on the equation of motion where the drag acceleration has a quadratic dependence on the ICME relative speed. This is expected to be an appropriate parametrization in the collisionless solar-wind environment, where the drag is caused primarily by the emission of MHD waves (Cargill *et al.*, 1996; Owens and Cargill, 2004). The presented version of DBM provides explicit-form solutions for the Sun–Earth ICME transit time and the impact speed (*cf.* Section 2). This offers very easy handling and straightforward/prompt application in the real-time space-weather forecasting. In Section 3 we present an analysis of the DBM performances, applying the statistical and case-study approach. The advantages and drawbacks of DBM are discussed in Section 4. Finally, in the Appendix we present a public, DBM-based, online forecast tool.

2. The Model

2.1. Model Description

The DBM is based on the assumption that the dynamics of ICMEs is dominated by the MHD "aerodynamic" drag (Cargill *et al.*, 1996; Vršnak, 2001a; Owens and Cargill, 2004; Cargill, 2004; Vršnak *et al.*, 2004, 2010; Vršnak and Žic, 2007; Vršnak, Vrbanec, and Čalogović, 2008; Borgazzi *et al.*, 2009; Lara and Borgazzi, 2009), *i.e.*, that ICMEs which are faster than the ambient solar wind are decelerated, whereas those slower than solar wind are accelerated by the ambient flow (*cf.*, Gopalswamy *et al.*, 2000). In particular, we consider the quadratic form for the drag acceleration (*cf.*, Cargill, 2004 and references therein):

$$a = -\gamma(v - w)|v - w|, \tag{1}$$

where v is the instantaneous ICME speed and w is the ambient solar-wind speed. It is important to note that Equation (1) defines the instantaneous acceleration, *i.e.*, each quantity (a, v, and w) is a function of time, t. The drag parameter γ can be expressed as

$$\gamma = \frac{c_{\mathrm{d}} A \rho_{\mathrm{w}}}{M + M_{\mathrm{v}}}, \tag{2}$$

where c_d is the dimensionless drag coefficient (Cargill, 2004), A is the ICME cross-sectional area, ρ_w is the ambient solar-wind density, and M is the ICME mass. The so called virtual mass, M_v, can be expressed approximately as $M_v \sim \rho_w V/2$, where V is the ICME volume (for details see, *e.g.*, Cargill, 2004 and references therein). Thus, taking into account $M = \rho V$, where ρ is the ICME density, the parameter γ can be expressed also as

$$\gamma = \frac{c_d A \rho_w}{V(\rho + \frac{\rho_w}{2})} = \frac{c_d}{L(\frac{\rho}{\rho_w} + \frac{1}{2})}, \tag{3}$$

where L is the thickness of the ICME in the radial direction, and we approximated $V \sim AL$. Equation (3) shows that in the limit $\rho_w \gg \rho$ the parameter γ does not depend on the solar-wind density ($\gamma = 2c_d/L$). On the other hand, in the regime $\rho \gg \rho_w$ the virtual mass becomes negligible and one finds $\gamma = c_d \rho_w/L\rho$, also meaning that γ becomes much smaller than in the $\rho_w \gg \rho$ case.

For the matter of illustration, let us consider the $\rho \gg \rho_w$ regime and assume that the CME is ten times denser than the ambient solar wind. Taking that at typical coronagraphic distances the CME radial thickness is on the order of one solar radius, say, 10^6 km, for $c_d = 1$ one finds $\gamma \sim 10^{-7}$ km^{-1}.

Generally, the value of γ changes with distance, so it is also dependent on time implicitly. Thus, the equation of motion reads

$$\frac{d^2 r}{dt^2} = -\gamma(r)\left(\frac{dr}{dt} - w(r)\right)\left|\frac{dr}{dt} - w(r)\right|, \tag{4}$$

where r is the heliospheric distance of the ICME leading edge. In general, Equation (4) has to be solved numerically (Vršnak and Žic, 2007).

Equation (4) is fully specified only if the dependencies $\gamma(r)$ and $w(r)$ are defined. This implies that we have to specify $A(r)$, $\rho_w(r)$, $M(r)$, and $c_d(r)$. In the simplest form of the model (which is used hereinafter) we assume that at sufficiently large distances (say, $r > 20r_\odot$, where $r_\odot$ is the solar radius) the following approximations are valid: $A \propto r^2$, $\rho_w \propto 1/r^2$, $M = $ const., and $c_d = $ const. (for details, see Cargill, 2004). Furthermore, we assume $\rho \gg \rho_w$, *i.e.*, we consider the case when the effect of the virtual mass M_v is negligible. Under such assumptions we get $\gamma(r) = $ const. (note that Vršnak and Gopalswamy, 2002 considered also the case $\gamma(r) \neq $ const.). Moreover, by taking into account the equation of continuity for the isotropic flow, the condition $\rho_w \propto 1/r^2$ implies also $w = $ const. (for details see, Vršnak *et al.*, 2004; Vršnak and Žic, 2007). In such a case, Equation (4) can be solved analytically (Vršnak *et al.*, 2004). Note that the approximation $w = $ const. for $r > 20r_\odot$ is consistent with the empirical solar-wind speed models proposed by Sheeley *et al.* (1997) and Leblanc, Dulk, and Bougeret (1998). The approximation $A \propto r^2$ is consistent with the fact that at typical coronagraphic distances the CME angular width remains constant, *i.e.*, that CME expands in a "self-similar" manner.

For the matter of illustration, let us consider the CME sample employed by Vršnak, Vrbanec, and Čalogović (2008), where masses were in the range $M \sim 10^{12} - 10^{13}$ kg. Employing a typical limb-CME angular width of $\phi = 60° \sim 1$ rad (Vršnak *et al.*, 2007), and applying the cone model (Zhao, Plunkett, and Liu, 2002), one finds that at $r = 20r_\odot$ the cross-sectional area is $A = (r\phi/2)^2\pi \sim 10^{20}$ m^2. Using $c_d = 1$ and a typical solar-wind density of $n \sim 10^9$ m^{-3} for this distance range (Leblanc, Dulk, and Bougeret, 1998), we find $\gamma \sim 0.2 - 2 \times 10^{-7}$ km^{-1}, consistent with the previous estimate based on Equation (3).

The analytical solutions of Equation (4), with the approximation $\gamma(r) = $ const. and $w(r) = $ const., read

$$v(t) = \frac{v_0 - w}{1 \pm \gamma(v_0 - w)t} + w, \tag{5}$$
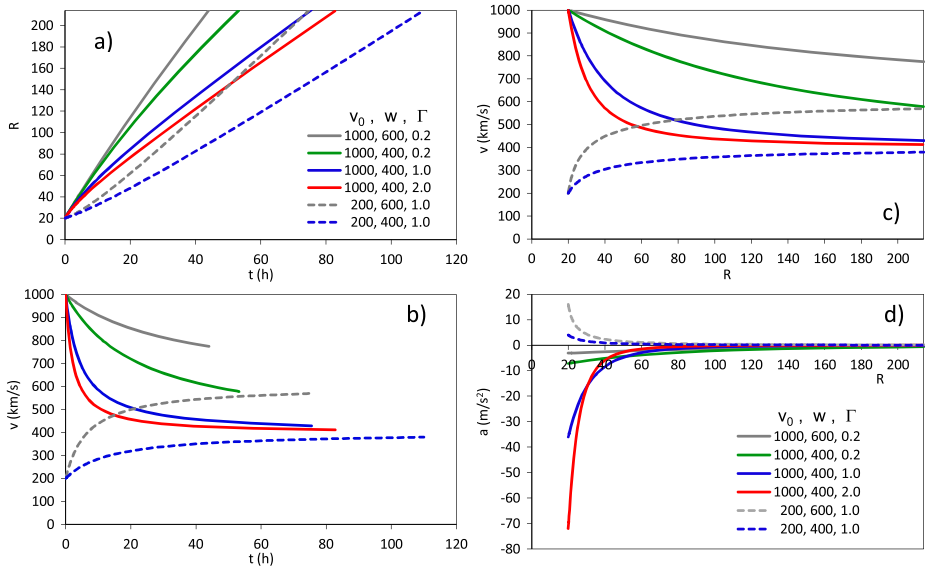
Figure 1 Examples of ICME kinematics based on DBM; the initial heliocentric distance is set to $r = 20r_{\odot}$ ($R = 20$). (a) Heliocentric distance *versus* time; (b) ICME speed *versus* time; (c) ICME speed *versus* distance; (d) ICME acceleration *versus* distance. The applied parameters are written in the legends in (a) and (d), where v_0 and w are expressed in km s^{-1} and $\Gamma = \gamma \times 10^7$ km^{-1} (*i.e.*, $\gamma = \Gamma \times 10^{-7}$ km^{-1}).

and

$$r(t) = \pm \frac{1}{\gamma} \ln\left[1 \pm \gamma(v_0 - w)t\right] + wt + r_0, \tag{6}$$

where $\pm$ depends on deceleration/acceleration regime, *i.e.*, it is plus for $v_0 > w$, and minus for $v_0 < w$.

Thus, in the simplest option of DBM, the solution of Equation (4) can be presented in the form $r(t)$, $v(t)$, or $v(r)$ explicitly. From this we can find the time T needed for an ICME to travel from a given initial ($t = 0$) radial distance, r_0, to 1 AU, for a given initial speed ("take-off speed"), $v_0 = v_{t=0} \equiv v_{r=r_0}$. In addition, the function $v(r)$ provides the "impact speed", v_1, *i.e.*, the ICME speed at 1 AU.

We have compared the analytical solutions for $\gamma = $ const. and $w = $ const. with the numerical outcome for $\gamma(r) \neq $ const. and $w(r) \neq $ const., where we employed the interplanetary density model proposed by Leblanc, Dulk, and Bougeret (1998) (for details, see Vršnak *et al.*, 2010). The comparison shows that the difference becomes very small beyond $r \sim 20r_{\odot}$; the deviations in the calculated transit times are generally within 1 h, which is much smaller than the uncertainties introduced by the limited measurement accuracy of the input parameters.

In Figure 1 several examples of the ICME kinematics, calculated employing the analytical solutions given by Equations (5) and (6), are presented. The kinematics of fast ICMEs is illustrated for various values of γ by taking the take-off speed of $v_0 = 1000$ km s^{-1} (full lines), whereas slow ICMEs are represented using $v_0 = 200$ km s^{-1} (dashed lines). Furthermore, we consider propagation in a slow ($w = 400$ km s^{-1}) and fast ($w = 600$ km s^{-1}; gray lines) solar-wind environment.

Figure 1a shows the ICME heliocentric distance ($R \equiv r/r_{\odot}$) *versus* time. The ICME Sun–Earth transit time is defined by the intercept of the curves and the upper graph-boundary

set at $R = 214$. The ICME speed presented as a function of time is displayed in Figure 1b. The kinematical curves end at $R = 214$, so the x-coordinate of their endpoint defines the ICME speed at 1 AU. The graph showing the ICME speed *versus* distance is presented in Figure 1c. The 1 AU speed is defined by the intercept of the curves and the right graph-boundary, set at $R = 214$. Finally, in Figure 1d we show the ICME acceleration presented as a function of heliocentric distance.

Figures 1b and c show clearly the tendency of ICMEs to adjust to the solar-wind speed. The adjustment is faster under high-γ conditions, representing "light" ICMEs in a relatively dense solar wind. The transit times range from ~ 40 to ~ 110 h, grouping around ~ 80 h, consistent with the so called "Brueckner 80 h rule" (Brueckner *et al.*, 1998). Note that under the high-γ conditions an initially slow ICME, launched into fast solar wind, can have shorter transit time than an initially fast ICME launched into slow solar wind. Figure 1 also implies that the shortest transit times are achieved if a very fast ICME is launched into fast solar wind under low-γ conditions (massive/narrow ICME in low-density high-speed solar-wind stream). Finally, it should be emphasized that in the high-γ case the proposed simplest form of the model ($\gamma = $ const.) might not be fully appropriate, since in this regime the virtual mass might not be negligible, implying that γ changes with the distance.

Figure 1d reveals that most of acceleration/deceleration occurs close to the Sun, say, within $R \sim 20 - 40$). The calculated accelerations are compatible with typical accelerations measured in the SoHO/LASCO-C3 field-of-view (Vršnak, 2001a; Vršnak *et al.*, 2004; Vršnak, Vrbanec, and Čalogović, 2008). The mean accelerations over the distance range $R = 20 - 214$ are found to be within ± 2 m s^{-2} for ICMEs whose take-off speed is relatively close to the solar-wind speed. The deceleration goes up to -10 m s^{-2} for very fast ICMEs in slow solar wind under high-γ conditions. Such values are consistent with measurements presented by, *e.g.*, Gopalswamy *et al.* (2000, 2001) and Michałek *et al.* (2004).

2.2. Physical Limitations

The DBM in the form presented in this paper is a model which considers the ICME as an expanding body that propagates through an isotropic environment that spreads out at a constant speed. The $1/r^2$ fall-off of the ambient density, the assumption that the effective ICME cross-section increases as $A \propto r^2$, and the assumption of constant mass of ICME implies a constant value of the drag parameter γ. However, this assumption is valid only if also the dimensionless drag coefficient c_d is constant over the considered distance range. Yet, this might not be true (see, *e.g.*, Cargill, 2004), and thus the constant-γ approximation intrinsically affects the accuracy of the arrival-time and impact-speed predictions. Note that constant-γ approximation might also not be appropriate in the case of very tenuous ICMEs (see Section 2.1). Finally, although the approximation $A \propto r^2$ seems to be valid at typical coronagraphic distances, since the CME angular width remains constant, this might not be true at larger heliospheric distances. For example, Bothmer and Schwenn (1998) have found from statistical analysis of the *Helios*, *Voyager*, and *Pioneer* data, measured in the distance range of $0.3 - 4.2$ AU, that the radial sizes of ICMEs increase as $L \propto r^{0.78 \pm 0.1}$, whereas the proton density decreases as $N \propto r^{-2.4 \pm 0.3}$. Taking approximately $N \propto 1/AL$, this indicates that the cross-sectional area increases as $A \propto r^{1.6}$, thus slower than r^2. However, taking into account the data scatter, the r^2 behavior is still within the error-limits (note also that the approximation $N \propto 1/AL$ is very crude).

Another intrinsic drawback of the employed model is that the equation of motion contains solely the drag term, *i.e.*, it is assumed that the driving Lorentz force has already ceased at heights below the considered propagation distance range (for a discussion see, *e.g.*, Chen

and Kunkel, 2010 and references therein; for the observational aspect, see, *e.g.*, Vršnak, 2001b and Vršnak *et al.*, 2004). However, in some cases this might not be true, since sometimes it is observed that even fast CMEs (*i.e.*, CMEs that are faster than solar wind) still significantly accelerate beyond $R = 20$ (see, *e.g.*, Vršnak *et al.*, 2004). Certainly, such a prolonged action of the Lorentz force can lead to a wrong prediction of the arrival time and impact speed. This can be avoided by employing kinematical measurements based on STEREO observations, *i.e.*, by using a larger take-off distance r_0, where the Lorentz force becomes definitely negligible (Vršnak *et al.*, 2004).

Finally, the model considers a simplified background solar-wind structure, *i.e.*, it is assumed that all parts of the ICME are embedded in an isotropic flow, where the flow speed does not change with distance. However, during the ICME propagation the ambient regime might change, *e.g.*, a fast ICME might first propagate through the slow solar wind and then it can enter a fast solar-wind stream (for an analysis of such events see Temmer *et al.*, 2011). Furthermore, fast ICMEs can encounter slow ICMEs that were launched earlier in the same direction, or slow ICMEs might be "pushed" by fast ICMEs that were launched later (for the application of the model to such an event see Temmer *et al.*, 2012). In this respect also note that ICMEs are spatially quite extended objects, so most likely, there will always be a certain influence of the high-speed wind originating from polar coronal holes (see, *e.g.*, Odstrcil, Riley, and Zhao, 2004).

2.3. Model Input/Output

The basic observational input parameters for DBM are related to the coronagraphic observations of CMEs. In particular, it is required to specify the velocity v_0 when the CME was located at a given distance r_0. Preferably, r_0 should be around, or beyond, a radial distance of $r = 20r_\odot$, so that the conditions $\gamma = $ const. and $w = $ const. are approximately fulfilled.

Note that measurements of both r_0 and v_0 are burdened by projection effects (*e.g.*, Burkepile *et al.*, 2004; Schwenn *et al.*, 2005; Vršnak *et al.*, 2007; Michalek, Gopalswamy, and Yashiro, 2009). There are various methods which can improve, to a certain degree, the accuracy of the estimates of r_0 and v_0 (*e.g.*, Schwenn *et al.*, 2005; Xie, Ofman, and Lawrence, 2004 and references therein). The validation analysis presented in Section 3 shows that the procedure proposed by Schwenn *et al.* (2005) gives the best results in the statistical sense. However, the results are only slightly better than those obtained by applying plane-of-sky values for r_0 and v_0. Bearing in mind other uncertainties (Sections 2.2 and 3) as well as the accuracy of measurements, this implies it is sufficient to use the plane-of-sky values for the DBM input.

To complete the set of necessary input parameters, the drag parameter γ and the solar-wind speed w have to be specified. From the physical point of view, the value of γ can be estimated, *e.g.*, by using Equation (3). As an example, let us consider a CME that is several times denser than the surrounding corona, say $\rho/\rho_w = 5$, and that its radial thickness is somewhere between 1 and 10 solar radii, corresponding to thin up to thick flux-rope regimes. Substituting these values into Equation (3), one finds $\gamma \sim 2 - 0.2 \times 10^{-7}$ km^{-1}, respectively. Most reasonable combinations of ρ/ρ_w and L would fall within or close to this range. This range is consistent with the outcome of a statistical analysis of transit times applied to a set of CMEs presented in Section 3. The analysis shows that from a statistical point of view γ most often attains values in the range $2 \times 10^{-8} - 2 \times 10^{-7}$ km^{-1}.

To conclude, in the case of massive ICMEs (generally meaning bright CMEs in the coronagraphic images) γ should have a small value on the order of 10^{-8} km^{-1}, whereas in the case of low-density ICMEs (dim in coronagraphic images) it should be closer to the upper limit, *i.e.*, 2×10^{-7} km^{-1}.

Table 1 Examples illustrating how the choice of parameter γ and the solar-wind speed w affects the DBM-calculated transit time T and the impact speed v_1.

γ [10^{-7} km^{-1}]	w [km s^{-1}]	T [h]	v_1 [km s^{-1}]
0.5	500	55	584
1.0	500	61	542
2.0	500	66	520
1.0	600	52	647
1.0	500	61	542
1.0	400	74	435

Considering the solar-wind speed, it is important to note that, generally, it depends on the location and time. However, in the simplest form of the DBM, we assume that the solar-wind speed is isotropic and constant. Thus, the straightforward option would be to use a typical slow solar-wind speed of 400 km s^{-1}, or somewhat lower, say 300 km s^{-1} in the period of deep solar minimum. Yet, if there is an equatorial coronal hole in the vicinity of the ICME source region, one should apply a higher value, say 500 – 600 km s^{-1}, since most likely, the ICME would be propagating at least partly through a high-speed solar-wind stream (HSS). In such a case, a high value of the solar-wind speed should be combined with a low value of γ since HSSs are characterized by low density. To check the possibility for interaction of the ICME with a HSS, it would be good to consult some of the numerical models that simulate the background solar wind (for details, see Temmer *et al.*, 2011).

According to the statistical analysis presented in Section 3, the most appropriate input values for the solar-wind speed should be within the range 300 – 600 km s^{-1}, and in the statistical sense, the best results are obtained for $w = 500$ km s^{-1}. In this respect, let us note that we have performed also a similar statistical analysis where we used the solar-wind speed based on the *in-situ* measurements at the time of the ICME take-off. This approach resulted in practically the same (even somewhat worse) statistical outcome regarding the accuracy of "predicted" transit times.

To illustrate the effect of different input values for γ and w, let us consider as an example an ICME which had a take-off speed of $v_0 = 1000$ km s^{-1} at $R_0 = 20$. The DBM-results for different combinations of γ and w are displayed in Table 1 (see also Figure 1). The first three rows show the results for $w = 500$ km s^{-1}, and different values of γ. Inspecting the results, one finds an uncertainty for the travel time of $\delta T \sim \pm 5$ h, and for the impact speed $\delta v_1 \sim \pm 30$ km s^{-1}. In the bottom three rows, the outcome for $\gamma = 1 \times 10^{-7}$ km^{-1} and various values of w is shown. For the travel time, one finds an uncertainty of $\delta T \sim \pm 10$ h, and for the impact speed $\delta v_1 \sim \pm 100$ km s^{-1}. The presented examples illustrate how important it is to check if there was a coronal hole in the vicinity of the CME source region, *i.e.*, if the ICME motion would be affected by a high-speed solar-wind stream.

Note that the output values, *i.e.*, the Sun–Earth transit time T and the 1 AU speed v_1, concern the front boundary of the ejection (for the relation between white-light and *in-situ* observations and related nomenclature see Rouillard, 2011), *i.e.*, the ICME-associated shock should arrive several hours before the ejection itself, depending on the size and Mach number of the ejection (see, *e.g.*, Russell and Mulligan, 2002). Furthermore, we emphasize that the present form of DBM does not take into account the direction of the ICME motion, *i.e.*, in the case of flank-encounter the arrival time at the Earth might be delayed for several hours, in extreme cases up to one, or even two days. The corresponding impact speeds for hits by the ejecta flank may be 100 to 200 km s^{-1} slower than for the apex-hit, if a self-similar expanding circular geometry for the ejection boundary is assumed. Derivations and plots for

these corrections and an application of such a geometry to STEREO/SECCHI observations are presented by Möstl and Davies (2012) and Davies *et al.* (2012). The application of this method to DBM will be presented in a separate paper.

3. Validation

In this section we test the performance of the model. First, in Section 3.1 we apply the model to a statistical sample of CME/ICME pairs, in order to check if the previously estimated ranges of values for w and γ are consistent with observations. Furthermore, we try to infer what combination of w and γ would provide the best prediction characteristics in the statistical sense, since for a given CME it is difficult to obtain a reliable observational input for a direct physics-based estimate of both w and γ. Finally, this section provides an insight into the accuracy of predictions from the statistical point of view. Then, in Section 3.2 we apply the model to several ICMEs to illustrate that the DBM is capable of reproducing the Sun–Earth kinematics of ICMEs, *i.e.*, that calculated "trajectories" are consistent with the observed ones.

3.1. Statistical Approach

In order to test the model from the statistical point of view, we employed the sample of 91 Sun–Earth events prepared by Schwenn *et al.* (2005) and the 30-event sample prepared by Manoharan (2006). Note that we consider only the arrival of the front boundary of the ejecta (not the ICME-driven shock).

First, we consider analytical solutions of Equation (4), valid in the approximation $\gamma(r) =$ const. and $w(r) =$ const. and providing explicit expressions for $v(t)$ and $r(t)$, as given by Equations (5) and (6). After substituting $v(t) = v(T) \equiv v_1$ and $r(t) = r(T) \equiv r_1$, and $t = T$, we get two algebraic equations with unknowns γ and w. Unfortunately, they cannot be solved analytically, to provide explicit forms for γ and w as a function of the observable parameters r_0, v_0, v_1, and T, *i.e.*, they have to be solved numerically.

Equations (5) and (6) can be rewritten as

$$\gamma = \frac{v_0 - v_1}{(v_0 - w)(v_1 - w)T} \tag{7}$$

and

$$\frac{E(w)}{\gamma} + wT + r_0 - r_1 = 0, \tag{8}$$

where we abbreviated

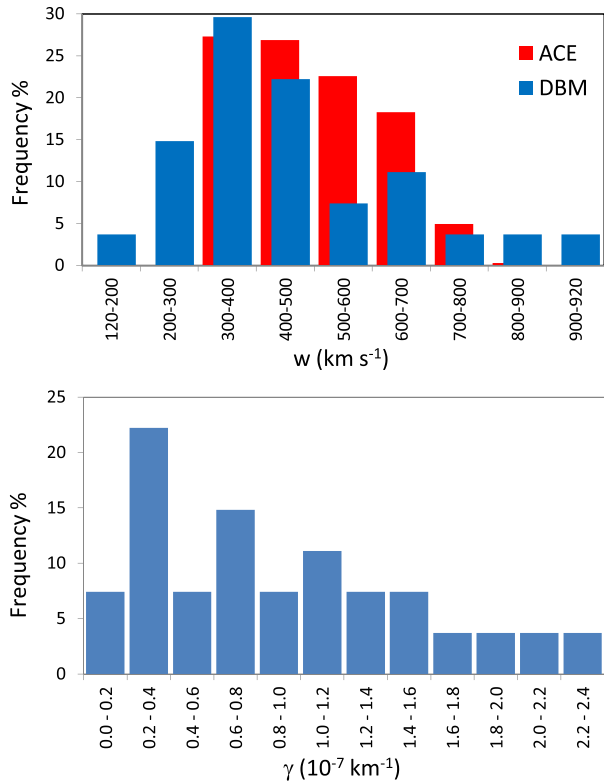$$E(w) = \ln\left[\frac{(v_0 - v_1)(v_0 - w)}{(v_1 - w)(v_0 + w)} + 1\right]. \tag{9}$$

After substituting γ from Equation (7) into Equation (8) one finds

$$F(w) \equiv \frac{(v_1 - w)(v_0 - w)T}{v_0 - v_1}E(w) + wT + r_0 - r_1 = 0. \tag{10}$$

Thus, the specific value $w(r_0, r_1, v_0, v_1, T)$ can be found by identifying w for which $F(w) = 0$. Once the value of w is evaluated, the drag parameter γ can be calculated employing Equation (7).

In Figure 2 we present the distribution of values of the solar-wind speed w and the drag parameter γ, obtained by employing the data provided by Schwenn *et al.* (2005) and

Manoharan (2006). Note that in a certain fraction of cases the solution $w(r_0, r_1, v_0, v_1, T)$ does not exist due to the incompatibility of the input values and the function ln appearing in Equation (9), *i.e.*, for those combinations of v_0 and v_1 for which the term in the square-brackets in Equation (9) is negative for any value of w.

The mean values for the distributions shown in Figure 2 are $\gamma = (1 \pm 0.6) \times 10^{-7} \text{ km}^{-1}$ and $w = 470 \pm 190 \text{ km s}^{-1}$. Median values are $0.8 \times 10^{-7} \text{ km}^{-1}$ and 410 km s^{-1}, respectively. In the upper panel of Figure 2, the inferred distribution of solar-wind speeds is compared with the distribution of "CMEless" solar-wind speeds based on the *in-situ* measurements in the period of low ICME activity in 2005 (day of the year $25 - 125$; for details see Vršnak, Temmer, and Veronig (2007) and Temmer, Vršnak, and Veronig (2007)). The overall pattern of the two distributions is similar, having the majority of speeds in the range $300 - 700 \text{ km s}^{-1}$. However, the DBM-distribution shows an excess in the high-velocity tail of the distribution, and even more pronounced overabundance on the low-velocity side. This "smearing" of the DBM-distribution could be attributed to inaccurate CME input parameters used in inferring the solar-wind speeds. Bearing in mind this drawback of the applied procedure, we conclude that the inferred distribution is quite consistent with the real solar-wind distribution.

Interestingly, no correlation is found between γ and w. This might be a somewhat surprising result since the solar-wind speed and density are anticorrelated, so one would expect also that w and $\gamma \propto \rho_w$ (see Equation (2)) are anticorrelated. Most likely, the $\rho_w(w)$ anticorrelation is masked by a large range of CME masses involved in the sample as well as
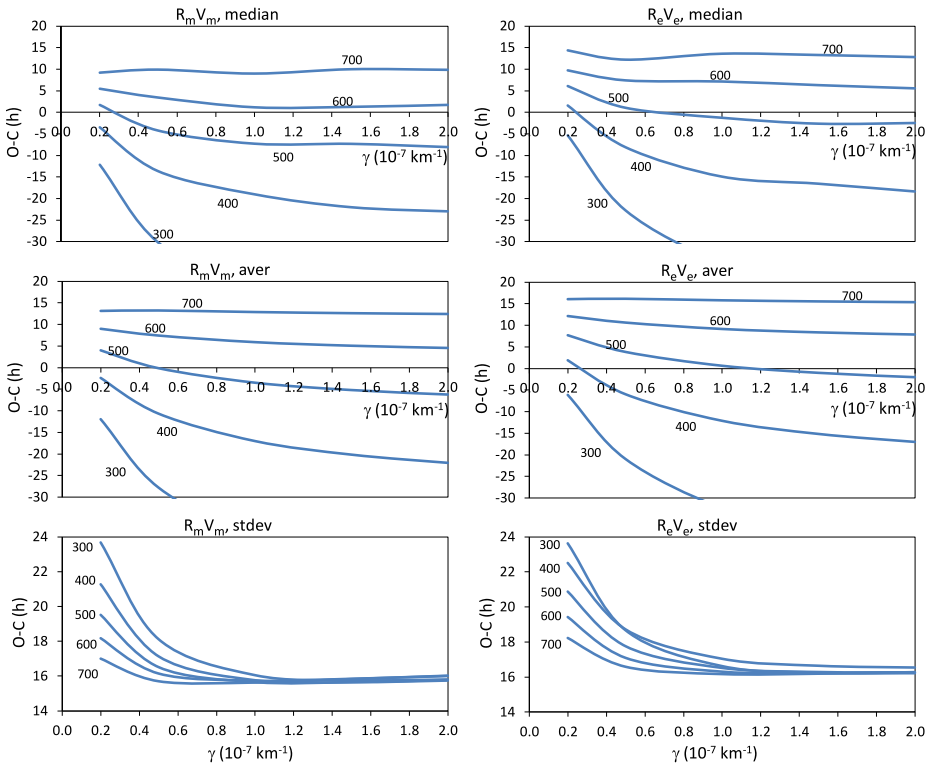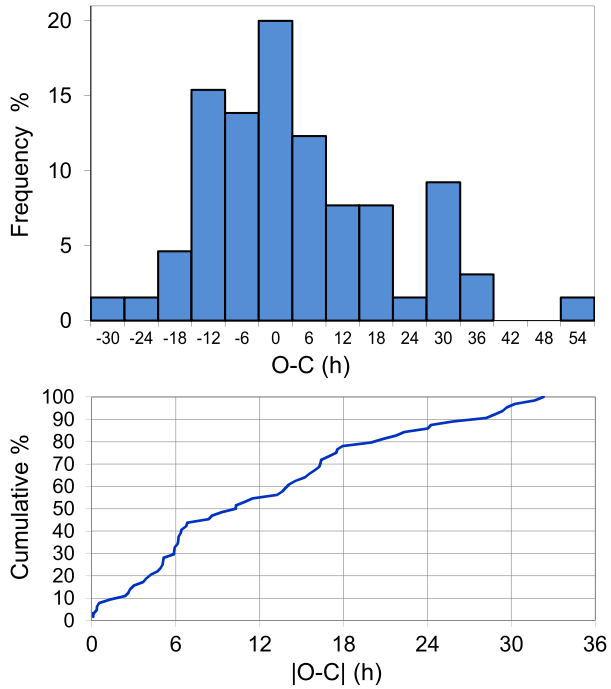
Figure 3 Analysis of the difference between observed and calculated travel times ($O - C$). In the left panels mean radial distance and speed (R_{m}, V_{m}) of the CME in the LASCO field-of-view are used as input values. The right panels show the outcome for the radial distance and speed at the moment of the last observation (R_{e}, V_{e}). The top panels represent median values, middle panels average values, and the bottom panels standard deviations. The applied values of the solar-wind speed w, expressed in $\mathrm{km\,s}^{-1}$, are written next to the curves.

a spectrum of CME sizes, implying also wide range of CME densities (see Equations (2) and (3)).

It should be also noted that the distribution of values of γ in Figure 2 is asymmetric, inclined towards the lower-value side. We have checked the CME masses determined from the coronagraphic data (compiled in the online LASCO CME Catalog; http://cdaw.gsfc.nasa.gov/CME_list/, for details see Yashiro *et al.* (2004)), and we found that the mean mass of the CMEs employed in the analysis was around four times higher than average (considering the lognormal distribution, the geometrical mean is even seven times larger). This explains the asymmetry since for more massive CMEs/ICMEs, the value of γ becomes lower (Equation (2)). Note that, generally, the distribution of values of γ is consistent with the range of values estimated on the "physics-based" approach in Section 2.

In the next step we used the CME/ICME sample from Schwenn *et al.* (2005) and calculated the "predicted" arrival time for each event using different combinations of γ and w, in the range from 2×10^{-8} to 2×10^{-7} km^{-1} and from 300 to 700 $\mathrm{km\,s}^{-1}$, respectively. Then, the calculated travel times (C) were compared with the observed ones (O), and the difference $O - C$ was determined. Note that we consider only the arrival of the ICME leading edge (*i.e.*, not the shock).

Figure 4 Top: Distribution of $O - C$ values for $\gamma = 10^{-7}$ km^{-1} and $w = 500$ km s^{-1}, applied to R_e, V_e data. Bottom: a corresponding cumulative distribution of $|O - C|$.

For each of the applied combinations of γ and w we checked the distributions of $O - C$ values, to find those combinations for which the average value of $O - C$ becomes zero. The results are summarized in Figure 3 where we show median values, average values and standard deviations (from top to bottom, respectively) of the $O - C$ distributions as a function of γ for different values of w. In the left panels mean radial distance and speed (R_m, V_m) of the CME in the LASCO field-of-view are used as the input values. The right panels show the outcome for the radial distance and speed at the moment of the last LASCO observation (R_e, V_e).

Inspecting Figure 3 one finds that average or median values of $O - C$ become zero for different combinations of γ and w. For example, considering the "R_m, V_m" option, one finds that if $w = 500$ km s^{-1} is assumed, the average $O - C$ becomes zero for $\gamma \sim 0.5 \times 10^{-7}$ km^{-1} (see middle-left panel). Assuming $w = 400$ km s^{-1} one gets $\gamma \sim 0.15 \times 10^{-7}$ km^{-1}, whereas assuming $w = 600$ km s^{-1} the corresponding value of γ becomes much higher than values allowed by the "physics-based" range of values estimated in Section 2. On the other hand, note that for, *e.g.*, $w = 500$ km s^{-1}, a combination with any γ in the range $\sim 0.2 - 1.5 \times 10^{-7}$ km^{-1} would result in average $O - C$ in the range $\sim \pm 5$ h. Bearing in mind that we used a relatively limited sample of events, and possible statistical fluctuations, all such combinations should also be possible/satisfactory. Thus, the choice of γ does not affect too much the results from a statistical point of view, *i.e.*, the solar-wind speed seems to be the more important parameter. This is consistent with the results presented by Vršnak and Žic (2007), which showed that the ambient solar-wind speed appears to be the most important factor in determining the ICME transit time. The probable reason lies in the fact that in most ICMEs the speeds become close to the solar-wind speed already relatively close to the Sun, whereas very massive ICMEs, where the adjustment to

the solar-wind speed is prolonged to larger distances, are relatively rare and do not affect significantly the statistical results.

On the other hand, standard deviations, *i.e.*, the dispersion of the $O - C$ values significantly increases for small values of γ. Standard deviations "stabilize" around the value of 16 h for $\gamma \geq 10^{-7}$ km^{-1}. For $\gamma = 10^{-7}$ km^{-1} one finds that the appropriate value of the solar-wind speed is $w \sim 500 - 550$ km s^{-1}. If higher values of γ are assumed, also the value of w increases. Note that the combination $\gamma = 1 \times 10^{-7}$ km^{-1} and $w = 500$ km s^{-1} is roughly consistent with the results presented in Figure 2.

The distribution of $O - C$ values for the combination $\gamma = 1 \times 10^{-7}$ km^{-1} and $w = 500$ km s^{-1}, for the R_e, V_e input option, is presented in Figure 4. The extreme delay at the right-hand-side of the distribution shown in the top panel of Figure 4 is almost surely due to a wrong CME/ICME-pair identification, since the delay is larger than two days. The distribution peaks at $O - C = 0$ (as requested), and has a standard deviation of 16 h. The standard deviation decreases to 15 h if the mentioned outlier is excluded.

In the bottom panel of Figure 4 we show the cumulative distribution of $|O - C|$, where we have excluded the previously mentioned outlier. The mean value of $|O - C|$ equals ~ 12 h. The distribution shows that ~ 55 % of events have $|O - C| < 12$ h and more than 85 % of events have $|O - C| < 1$ day. If we restrict the sample only to events where $R_e > 15$ or $R_e > 20$ the average $|O - C|$ decreases to below 12 h. However, the shape of the cumulative distribution does not change significantly, except that now ~ 60 % of events have $|O - C| < 12$ h and ~ 90 % have $|O - C| < 1$ day. In this respect it is important to discuss/resolve what means a "successful prediction", since the obtained standard deviations of $15 - 16$ h, as well as the mean value $|O - C| \sim 12$ h, are relatively large. Yet, $O - C$ deviations become significantly smaller when fast CMEs (short transit times) are considered, especially if CMEs are launched from regions close to the solar disc center. Note that this subset of events tends to be more geoeffective, thus for purposes of space-weather forecasting one can count on better accuracy of predictions (this statistically very demanding study will be presented in a separate paper).

The procedure described above was repeated for the sample from Schwenn *et al.* (2005) using also the mean speed in the LASCO field-of-view (V_m) as well as the deprojected value (denoted as "radial" in Schwenn *et al.*, 2005). We also employed the samples from Manoharan (2006) and Zhang *et al.* (2003). All of these options led to similar results, in statistical sense not significantly different from those presented in Figure 4.

3.2. Tracking the Interplanetary Kinematics

To test the capabilities of DBM in more detail, we have performed a number of case studies, where we compared the deprojected kinematics of ICMEs reconstructed from remote-sensing observations by the STEREO spacecraft with the kinematics calculated by DBM. In Figure 5, the deprojected kinematics of three ICMEs are shown as typical examples. For the first two events (CMEs launched on 15 November 2007 and 12 December 2008, respectively) we employ the measurements presented by Liu *et al.* (2010). The November 2007 event was analyzed also by Rouillard *et al.* (2010) and Farrugia *et al.* (2011), and the December 2008 event by Davis *et al.* (2009). For the third event, tracked by the STEREO spacecraft over the full Sun–Earth distance range (CME launched on 1 June 2008) we use the measurements presented in detail by Rollett *et al.* (2012) and Temmer *et al.* (2011).

The ICME of 15 November 2007 was characterized by a low take-off speed, and was continuously accelerating towards the velocity of $500 - 600$ km s^{-1}. The DBM kinematics reproduces the observations in the best way by applying the asymptotic solar-wind speed
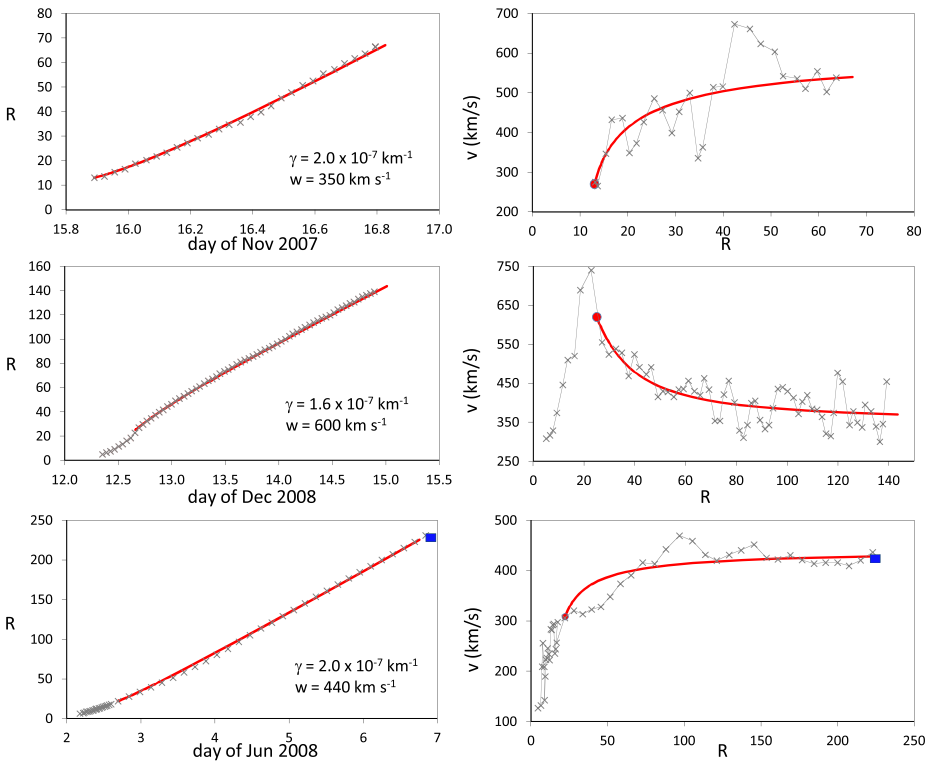
Figure 5 Heliospheric kinematics of three ICMEs, launched on 15 November 2007 (top), 12 December 2008 (middle), and 1 June 2008 (bottom). Left panels show the deprojected distance *versus* time, whereas right panels show the deprojected speed *versus* distance. Observations are drawn in gray, whereas the red line shows the calculated kinematics (parameters are written in the legend). Blue squares in the bottom graphs represent *in-situ* measurements.

of $w = 600 \text{ km s}^{-1}$ and $\gamma = 1.6 \times 10^{-7} \text{ km}^{-1}$. Indeed, the CME was launched from a region surrounded by an equatorial coronal hole that was a source of a high-speed solar-wind stream. Furthermore, in the SoHO/LASCO catalogue (http://cdaw.gsfc.nasa.gov/CME_list/, see Yashiro *et al.*, 2004) the event was classified as "Poor Event", implying that this was a low-mass CME, explaining the rather large value of γ.

The ICME of 12 December 2008 was accelerating rapidly up to $R \sim 23$, to achieve a relatively high take-off speed of $v \sim 740 \text{ km s}^{-1}$, after which it started to decelerate. The decelerated propagation can be reproduced very closely by DBM, applying $\gamma = 2.0 \times 10^{-7} \text{ km}^{-1}$ and $w = 350 \text{ km s}^{-1}$. Again, the event was classified in the SoHO/LASCO catalogue as "Poor Event", consistent with a relatively high value of γ. There were no equatorial coronal holes in the vicinity of the eruption, which explains the low asymptotic solar-wind speed w, and is in addition consistent with the high value of γ (slow solar wind is characterized by denser plasma flow). Note that in this event it would not be possible to predict the ICME arrival based on the LASCO data, since the CME was gradually accelerating up to large heights, whereas in LASCO the CME was followed only up to $R \sim 12$, where it had the speed of only $\sim 320 \text{ km s}^{-1}$. Thus, whenever possible, it would be the best to use the deprojected speeds from STEREO as input.

The propagation of the third ICME, launched on $1-2$ June 2008, was followed remotely beyond 1 AU, and was recorded *in situ* by STEREO-B (for details see Möstl *et al.*, 2009; Rollett *et al.*, 2012, and Temmer *et al.*, 2011). The event was first studied by Robbrecht, Patsourakos, and Vourlidas (2009) who classified it as "stealth CME" having no recognizable signatures of associated low-coronal activity. Various aspects of the event were also analyzed by Möstl *et al.* (2009), Lynch *et al.* (2010), and Wood, Howard, and Socker (2010). The remotely measured heliospheric kinematics presented in Figure 5 is based on the harmonic mean method (Howard and Tappin, 2009; Lugaz, Vourlidas, and Roussev, 2009), modified in such a way as to follow the ICME segment that propagates towards the *in-situ* observer (for details see Möstl *et al.*, 2010; Rollett *et al.*, 2012; Temmer *et al.*, 2011, and references therein). As seen from the bottom graphs of Figure 5, the DBM with $w = 440$ km s^{-1} and $\gamma = 2 \times 10^{-7}$ km^{-1} reproduces quite well the remotely measured kinematics as well as the *in-situ* measurements. The applied solar-wind speed is consistent with the modeled solar-wind structure (for details see Temmer *et al.*, 2011). Furthermore, the LASCO data show that the CME was rather dim, consistent with the relatively high value of γ.

Finally, we emphasize that the relationship between the white-light observations and the *in-situ* measurements is not trivial (Rouillard, 2011). In fast/bright ICMEs, the white-light leading edge probably depicts the compressed shock-sheath region, whereas in slow shockless ICMEs the situation is less clear. Here, we have adjusted the DBM input parameters to fit the kinematics of the ICME leading edge, assuming that the ICME expands in a self-similar manner and that the sheath region is not very thick, *i.e.*, that the propagation of the white-light leading edge is not much different from the propagation of the ejection itself. Of course, this is a very crude approximation, but our intention was just to illustrate that the overall shape of kinematical curves can be reproduced well by the DBM. A more detailed analysis of the herein employed ICMEs and several other events will be presented in a separate paper.

4. Conclusion

In this paper we presented a version of the drag-based model that provides analytical solutions for the ICME kinematics. This allows easy handling and prompt application in the real-time space-weather forecasting (see the Appendix). The model can be adjusted to various situations, *i.e.*, provides distinction between weak-drag or strong-drag effects as well as choosing between slow and fast solar-wind environment. However, in the present state it cannot account for ICME–ICME interactions, though it can help in the analysis and comprehension of such events (for an example see Temmer *et al.*, 2012). Another drawback is that using this (the simplest) version of the model, only the arrival of the front boundary of the ejecta can be predicted, *i.e.*, it does not account for the impact of the ICME-driven shock.

The application of the model to a statistical sample of events revealed that the drag parameter γ most often ranges between 2×10^{-8} km^{-1} and 2×10^{-7} km^{-1}, consistent with the physics-based estimates. The lower values are appropriate for massive ICMEs in fast solar-wind environment, characterized by a low density. High values apply to low-density ICMEs in the slow solar wind. This effect explains the asymmetry present in Figure 2, since the mean mass of the CMEs from the employed sample was considerably higher than average. The optimum value of the solar-wind speed, $w \sim 500$ km s^{-1}, can be explained by a large spatial extent of ICMEs, so their kinematics are at least partly affected by the fast wind from polar coronal holes. Furthermore, at least a fraction of ICMEs propagate interacting with high-speed solar-wind streams from equatorial coronal holes, which also increases the average value of w.

The validation analysis showed that the expected typical errors in predicting the arrival times of ICMEs by the presented version of the model is around 0.5 days. We believe that the distribution of errors can be significantly reduced by taking the previously mentioned drawbacks into account. We will focus on these aspects when developing a more advanced version of the model. Finally, we demonstrated that the measured heliospheric ICME kinematics can be reproduced by the model, at least for isolated events propagating in a simple solar-wind environment. Yet, as shown by Temmer *et al.* (2011, 2012) the ICME propagation can be much more complex in situations when the ambient solar-wind regime changes, or for the events which include ICME–ICME interaction.

Appendix

Hereinafter, we present an open-access online forecast tool for predicting the ICME arrival at 1 AU, which is based on the previously described formulation of the DBM. This forecast tool was developed in the frame of the European Commission FP7 Project SOTERIA (SOlar-TERrestrial Investigations and Archives; www.soteria-space.eu) and advanced

Figure 6 Input page of the Drag-Based Model forecast web-site, available at: http://oh.geof.unizg.hr/CADBM/cadbm.php.

Forecasting the Arrival of ICMEs at 1 AU: The Drag-Based Model

Full description about the calculation method you can find here. 📄

Output:

CME arrival date & time at 1AU: **2012-2-24 13h:5min**
Travel time (1AU): **61.08** h
Transit distance in R_s: **214** R_s
Transit speed (at 214 R_s): **542** km/s

Input parameters:

CME take-off date & time: **2012-2-22 0h:0min**
R_0=20 R_s, v_0=1000 km/s, γ=1×10^{-7} km^{-1}, w=500 km/s

Calculated in 0.12 seconds.

CME start date:	Feb 22 2012 📅
CME start time:	00 h 00 min
R_0 - starting radial distance of CME (R_s)	20
v_0 - speed of CME at R_0 (km/s)	1000
γ - drag parameter (10^{-7} km^{-1})	1
w - asymptotic solar wind speed (km/s)	500

Calculate   Reset!

Figure 7   Output page of the DBM forecast web-site.

within FP7 Project COMESEP (COronal Mass Ejections and Solar Energetic Particles; www.comesep.eu). The tool is available at http://oh.geof.unizg.hr/CADBM/cadbm.php.

The input page of the DBM forecast web-site is presented in Figure 6. In the first two input boxes the user has to specify the date and time (UT) when the CME was located at a given distance R_0 (third input box). Preferably, R_0 should be around, or beyond, the radial distance of $R \sim 20$. Finally, the CME speed at R_0, $v_0 \equiv v(R_0)$, is required (fourth input box). The default values are set to $R = 20$ and $v_0 = 1000 \text{ km s}^{-1}$.

To complete the set of input parameters, the drag parameter γ (expressed in 10^{-7} km^{-1}) and the solar-wind speed w (expressed in km s^{-1}) have to be specified, too. In Sections 2 and

3 it was shown that γ and w most often attain values in the range $2 \times 10^{-8} - 2 \times 10^{-7}$ km^{-1} and $300 - 600$ km s^{-1}, respectively. In the case of massive ICMEs (generally meaning bright CMEs in the coronagraphic images) γ should have a small value, whereas in the case of low-density ICME (dim in coronagraphic images) it should be closer to the upper limit. In the slow-wind environment, w should be chosen between 300 and 400 km s^{-1}. If there is an equatorial coronal hole in the vicinity of the ICME source region, one should apply a higher value, say, $500 - 600$ km s^{-1}. In such a case, a high value of solar-wind speed should be combined with a low value of γ, since the fast solar wind is characterized by a low density. Following the results presented in Section 3, the default values are set to $\gamma = 1 \times 10^{-7}$ km^{-1} and $w = 500$ km s^{-1}. For inexperienced users we would recommend that beside the default values of w and γ to use also the mentioned limiting combinations to estimate a time-window within which the ICME arrival is expected.

After clicking the "Calculate" button, the output page appears (Figure 7). The model output provides an estimate of the arrival date and time of the ICME at 1 AU, as well as the travel time from $R = R_0$ to $R = 214$ (=1 AU) and the impact speed v_1 at 1 AU. Beside the outcome of the calculation, the output page summarizes the input parameters used, as well as the a new input set, to provide a new calculation (see bottom part of Figure 7).

Again, we emphasize that the output values correspond to the front boundary of the ejecta, *i.e.*, the ICME-associated shock should arrive several hours earlier. Furthermore, the present form of DBM does not take into account the direction of the ICME motion, *i.e.*, in the case of flank-encounter the arrival time at the Earth might be delayed by several hours, in extreme cases up to one day. It is foreseen that in future a more advanced form of DBM will be developed, which will take these two effects into account.

References

Borgazzi, A., Lara, A., Echer, E., Alves, M.V.: 2009, Dynamics of coronal mass ejections in the interplanetary medium. *Astron. Astrophys.* **498**, 885 – 889. doi:10.1051/0004-6361/200811171.

Bothmer, V., Schwenn, R.: 1998, The structure and origin of magnetic clouds in the solar wind. *Ann. Geophys.* **16**, 1 – 24.

Brueckner, G.E., Howard, R.A., Koomen, M.J., Korendyke, C.M., Michels, D.J., Moses, J.D., Socker, D.G., Dere, K.P., Lamy, P.L., Llebaria, A., Bout, M.V., Schwenn, R., Simnett, G.M., Bedford, D.K., Eyles, C.J.: 1995, The large angle spectroscopic coronagraph (LASCO). *Solar Phys.* **162**, 357 – 402. doi:10.1007/BF00733434.

Brueckner, G.E., Delaboudiniere, J.-P., Howard, R.A., Paswaters, S.E., St. Cyr, O.C., Schwenn, R., Lamy, P., Simnett, G.M., Thompson, B., Wang, D.: 1998, Geomagnetic storms caused by coronal mass ejections (CMEs): March 1996 through June 1997. *Geophys. Res. Lett.* **25**, 3019 – 3022. doi:10.1029/98GL00704.

Burkepile, J.T., Hundhausen, A.J., Stanger, A.L., St. Cyr, O.C., Seiden, J.A.: 2004, Role of projection effects on solar coronal mass ejection properties: 1. A study of CMEs associated with limb activity. *J. Geophys. Res.* **109**, A03103. doi:10.1029/2003JA010149.

Byrne, J.P., Maloney, S.A., McAteer, R.T.J., Refojo, J.M., Gallagher, P.T.: 2010, Propagation of an Earth-directed coronal mass ejection in three dimensions. *Nature Comm.* **1**, 74. doi:10.1038/ncomms1077.

Cargill, P.J.: 2004, On the aerodynamic drag force acting on interplanetary coronal mass ejections. *Solar Phys.* **221**, 135 – 149. doi:10.1023/B:SOLA.0000033366.10725.a2.

Cargill, P.J., Chen, J., Spicer, D.S., Zalesak, S.T.: 1996, Magnetohydrodynamic simulations of the motion of magnetic flux tubes through a magnetized plasma. *J. Geophys. Res.* **101**, 4855 – 4870. doi:10.1029/95JA03769.

Chen, J., Kunkel, V.: 2010, Temporal and physical connection between coronal mass ejections and flares. *Astrophys. J.* **717**, 1105 – 1122. doi:10.1088/0004-637X/717/2/1105.

Cho, K.-S., Moon, Y.-J., Dryer, M., Fry, C.D., Park, Y.-D., Kim, K.-S.: 2003, A statistical comparison of interplanetary shock and CME propagation models. *J. Geophys. Res.* **108**, SSH8. doi:10.1029/2003JA010029.

Davies, J.A., Harrison, R.A., Perry, C.H., Möstl, C., Lugaz, N., Rollett, T., Davis, C.J., Crothers, S.R., Temmer, M., Eyles, C.J., Savani, N.P.: 2012, A self-similar expansion model for use in solar wind transient propagation studies. *Astrophys. J.* **750**, 23. doi:10.1088/0004-637X/750/1/23.

Davis, C.J., Davies, J.A., Lockwood, M., Rouillard, A.P., Eyles, C.J., Harrison, R.A.: 2009, Stereoscopic imaging of an Earth-impacting solar coronal mass ejection: a major milestone for the STEREO mission. *Geophys. Res. Lett.* **36**, L08102. doi:10.1029/2009GL038021.

Dryer, M., Smith, Z., Fry, C.D., Sun, W., Deehr, C.S., Akasofu, S.-I.: 2004, Real-time shock arrival predictions during the "Halloween 2003 epoch". *Space Weather* **2**, S09001. doi:10.1029/2004SW000087.

Falkenberg, T.V., Vršnak, B., Taktakishvili, A., Odstrcil, D., MacNeice, P., Hesse, M.: 2010, Investigations of the sensitivity of a coronal mass ejection model (ENLIL) to solar input parameters. *Space Weather* **8**, S06004. doi:10.1029/2009SW000555.

Falkenberg, T.V., Vennerstrom, S., Brain, D.A., Delory, G., Taktakishvili, A.: 2011, Multipoint observations of coronal mass ejection and solar energetic particle events on Mars and Earth during November 2001. *J. Geophys. Res.* **116**, A06104. doi:10.1029/2010JA016279.

Farrugia, C.J., Berdichevsky, D.B., Möstl, C., Galvin, A.B., Leitner, M., Popecki, M.A., Simunac, K.D.C., Opitz, A., Lavraud, B., Ogilvie, K.W., Veronig, A.M., Temmer, M., Luhmann, J.G., Sauvaud, J.A.: 2011, Multiple, distant (40 deg) *in situ* observations of a magnetic cloud and a corotating interaction region complex. *J. Atmos. Solar-Terr. Phys.* **73**, 1254–1269. doi:10.1016/j.jastp.2010.09.011.

Feng, X.S., Zhang, Y., Sun, W., Dryer, M., Fry, C.D., Deehr, C.S.: 2009, A practical database method for predicting arrivals of "average" interplanetary shocks at Earth. *J. Geophys. Res.* **114**, A01101. doi:10.1029/2008JA013499.

Fry, C.D., Dryer, M., Smith, Z., Sun, W., Deehr, C.S., Akasofu, S.-I.: 2003, Forecasting solar wind structures and shock arrival times using an ensemble of models. *J. Geophys. Res.* **108**, SSH5. doi:10.1029/2002JA009474.

González-Esparza, J.A., Lara, A., Pérez-Tijerina, E., Santillán, A., Gopalswamy, N.: 2003, A numerical study on the acceleration and transit time of coronal mass ejections in the interplanetary medium. *J. Geophys. Res.* **108**, SSH9. doi:10.1029/2001JA009186.

Gopalswamy, N., Lara, A., Lepping, R.P., Kaiser, M.L., Berdichevsky, D., St. Cyr, O.C.: 2000, Interplanetary acceleration of coronal mass ejections. *Geophys. Res. Lett.* **27**, 145–148.

Gopalswamy, N., Lara, A., Yashiro, S., Kaiser, M.L., Howard, R.A.: 2001, Predicting the 1-AU arrival times of coronal mass ejections. *J. Geophys. Res.* **106**, 29207–29218. doi:10.1029/2001JA000177.

Howard, T.A., Tappin, S.J.: 2009, Interplanetary coronal mass ejections observed in the heliosphere: 3. Physical implications. *Space Sci. Rev.* **147**, 89–110. doi:10.1007/s11214-009-9577-7.

Howard, R.A., Moses, J.D., Vourlidas, A., Newmark, J.S., Socker, D.G., Plunkett, S.P., Korendyke, C.M., Cook, J.W., Hurley, A., Davila, J.M., Thompson, W.T., St Cyr, O.C., Mentzell, E., Mehalick, K., Lemen, J.R., Wuelser, J.P., Duncan, D.W., Tarbell, T.D., Wolfson, C.J., Moore, A., Harrison, R.A., Waltham, N.R., Lang, J., Davis, C.J., Eyles, C.J., Mapson-Menard, H., Simnett, G.M., Halain, J.P., Defise, J.M., Mazy, E., Rochus, P., Mercier, R., Ravet, M.F., Delmotte, F., Auchere, F., Delaboudiniere, J.P., Bothmer, V., Deutsch, W., Wang, D., Rich, N., Cooper, S., Stephens, V., Maahs, G., Baugh, R., McMullin, D., Carter, T.: 2008, Sun Earth connection coronal and heliospheric investigation (SECCHI). *Space Sci. Rev.* **136**, 67–115. doi:10.1007/s11214-008-9341-4.

Jackson, B.V., Buffington, A., Hick, P.P., Altrock, R.C., Figueroa, S., Holladay, P.E., Johnston, J.C., Kahler, S.W., Mozer, J.B., Price, S., Radick, R.R., Sagalyn, R., Sinclair, D., Simnett, G.M., Eyles, C.J., Cooke, M.P., Tappin, S.J., Kuchar, T., Mizuno, D., Webb, D.F., Anderson, P.A., Keil, S.L., Gold, R.E., Waltham, N.R.: 2004, The solar mass-ejection imager (SMEI) mission. *Solar Phys.* **225**, 177–207. doi:10.1007/s11207-004-2766-3.

Koskinen, H.E.J., Huttunen, K.E.J.: 2006, Geoeffectivity of coronal mass ejections. *Space Sci. Rev.* **124**, 169–181. doi:10.1007/s11214-006-9103-0.

Lara, A., Borgazzi, A.I.: 2009, Dynamics of interplanetary CMEs and associated type II bursts. In: Gopalswamy, N., Webb, D.F. (eds.) *Proc. IAU Symp.* **257**, 287–290. doi:10.1017/S1743921309029421.

Leblanc, Y., Dulk, G.A., Bougeret, J.-L.: 1998, Tracing the electron density from the corona to 1 AU. *Solar Phys.* **183**, 165–180.

Liu, Y., Thernisien, A., Luhmann, J.G., Vourlidas, A., Davies, J.A., Lin, R.P., Bale, S.D.: 2010, Reconstructing coronal mass ejections with coordinated imaging and *in situ* observations: global structure, kinematics, and implications for space weather forecasting. *Astrophys. J.* **722**, 1762–1777. doi:10.1088/0004-637X/722/2/1762.

Lugaz, N., Vourlidas, A., Roussev, I.I.: 2009, Deriving the radial distances of wide coronal mass ejections from elongation measurements in the heliosphere – application to CME–CME interaction. *Ann. Geophys.* **27**, 3479–3488. doi:10.5194/angeo-27-3479-2009.

Lynch, B.J., Li, Y., Thernisien, A.F.R., Robbrecht, E., Fisher, G.H., Luhmann, J.G., Vourlidas, A.: 2010, Sun to 1 AU propagation and evolution of a slow streamer-blowout coronal mass ejection. *J. Geophys. Res.* **115**, A07106. doi:10.1029/2009JA015099.

Maloney, S.A., Gallagher, P.T.: 2010, Solar wind drag and the kinematics of interplanetary coronal mass ejections. *Astrophys. J. Lett.* **724**, L127 – L132. doi:10.1088/2041-8205/724/2/L127.

Manchester, W.B., Gombosi, T.I., Roussev, I., Ridley, A., De Zeeuw, D.L., Sokolov, I.V., Powell, K.G., Tóth, G.: 2004, Modeling a space weather event from the Sun to the Earth: CME generation and interplanetary propagation. *J. Geophys. Res.* **109**, A02107. doi:10.1029/2003JA010150.

Manoharan, P.K.: 2006, Evolution of coronal mass ejections in the inner heliosphere: a study using white-light and scintillation images. *Solar Phys.* **235**, 345 – 368. doi:10.1007/s11207-006-0100-y.

Manoharan, P.K.: 2010, Ooty interplanetary scintillation – remote-sensing observations and analysis of coronal mass ejections in the heliosphere. *Solar Phys.* **265**, 137 – 157. doi:10.1007/s11207-010-9593-5.

Manoharan, P.K., Mujiber Rahman, A.: 2011, Coronal mass ejections: propagation time and associated internal energy. *J. Atmos. Solar-Terr. Phys.* **73**, 671 – 677. doi:10.1016/j.jastp.2011.01.017.

Manoharan, P.K., Gopalswamy, N., Yashiro, S., Lara, A., Michalek, G., Howard, R.A.: 2004, Influence of coronal mass ejection interaction on propagation of interplanetary shocks. *J. Geophys. Res.* **109**, A06109. doi:10.1029/2003JA010300.

McKenna-Lawlor, S.M.P., Dryer, M., Smith, Z., Kecskemety, K., Fry, C.D., Sun, W., Deehr, C.S., Berdichevsky, D., Kudela, K., Zastenker, G.: 2002, Arrival times of flare/halo CME associated shocks at the Earth: comparison of the predictions of three numerical models with these observations. *Ann. Geophys.* **20**, 917 – 935. doi:10.5194/angeo-20-917-2002.

McKenna-Lawlor, S.M.P., Dryer, M., Kartalev, M.D., Smith, Z., Fry, C.D., Sun, W., Deehr, C.S., Kecskemety, K., Kudela, K.: 2006, Near real-time predictions of the arrival at Earth of flare-related shocks during Solar Cycle 23. *J. Geophys. Res.* **111**, A11103. doi:10.1029/2005JA011162.

McKenna-Lawlor, S.M.P., Dryer, M., Fry, C.D., Smith, Z.K., Intriligator, D.S., Courtney, W.R., Deehr, C.S., Sun, W., Kecskemety, K., Kudela, K., Balaz, J., Barabash, S., Futaana, Y., Yamauchi, M., Lundin, R.: 2008, Predicting interplanetary shock arrivals at Earth, Mars, and Venus: a real-time modeling experiment following the solar flares of 5 – 14 December 2006. *J. Geophys. Res.* **113**, A06101. doi:10.1029/2007JA012577.

Michalek, G., Gopalswamy, N., Yashiro, S.: 2009, Expansion speed of coronal mass ejections. *Solar Phys.* **260**, 401 – 406. doi:10.1007/s11207-009-9464-0.

Michałek, G., Gopalswamy, N., Lara, A., Manoharan, P.K.: 2004, Arrival time of halo coronal mass ejections in the vicinity of the Earth. *Astron. Astrophys.* **423**, 729 – 736. doi:10.1051/0004-6361:20047184.

Morrill, J.S., Howard, R.A., Vourlidas, A., Webb, D.F., Kunkel, V.: 2009, The impact of geometry on observations of CME brightness and propagation. *Solar Phys.* **259**, 179 – 197. doi:10.1007/s11207-009-9403-0.

Möstl, C., Davies, J.A.: 2012, Speeds and arrival times of solar transients approximated by self-similar expanding circular fronts. *Solar Phys.*, in press. doi:10.1007/s11207-012-9978-8.

Möstl, C., Farrugia, C.J., Temmer, M., Miklenic, C., Veronig, A.M., Galvin, A.B., Leitner, M., Biernat, H.K.: 2009, Linking remote imagery of a coronal mass ejection to its *in situ* signatures at 1 AU. *Astrophys. J. Lett.* **705**, L180 – L185. doi:10.1088/0004-637X/705/2/L180.

Möstl, C., Temmer, M., Rollett, T., Farrugia, C.J., Liu, Y., Veronig, A.M., Leitner, M., Galvin, A.B., Biernat, H.K.: 2010, STEREO and *Wind* observations of a fast ICME flank triggering a prolonged geomagnetic storm on 5 – 7 April 2010. *Geophys. Res. Lett.* **372**, L24103. doi:10.1029/2010GL045175.

Odstrcil, D., Pizzo, V.J., Arge, C.N.: 2005, Propagation of the 12 May 1997 interplanetary coronal mass ejection in evolving solar wind structures. *J. Geophys. Res.* **110**, A02106. doi:10.1029/2004JA010745.

Odstrcil, D., Riley, P., Zhao, X.P.: 2004, Numerical simulation of the 12 May 1997 interplanetary CME event. *J. Geophys. Res.* **109**, A02116. doi:10.1029/2003JA010135.

Oler, C.: 2004, Prediction performance of space weather forecast centers following the extreme events of October and November 2003. *Space Weather* **2**, S08001. doi:10.1029/2004SW000076.

Owens, M., Cargill, P.: 2004, Predictions of the arrival time of coronal mass ejections at 1 AU: an analysis of the causes of errors. *Ann. Geophys.* **22**, 661 – 671. doi:10.5194/angeo-22-661-2004.

Reiner, M.J., Kaiser, M.L., Bougeret, J.-L.: 2007, Coronal and interplanetary propagation of CME/shocks from radio, *in situ* and white-light observations. *Astrophys. J.* **663**, 1369 – 1385. doi:10.1086/518683.

Robbrecht, E., Patsourakos, S., Vourlidas, A.: 2009, No trace left behind: STEREO observation of a coronal mass ejection without low coronal signatures. *Astrophys. J.* **701**, 283 – 291. doi:10.1088/0004-637X/701/1/283.

Rollett, T., Möstl, C., Temmer, M., Veronig, A.M., Farrugia, C.J., Biernat, H.K.: 2012, Constraining the kinematics of coronal mass ejections in the inner heliosphere with *in-situ* signatures. *Solar Phys.* **276**, 293 – 314. doi:10.1007/s11207-011-9897-0.

Rouillard, A.P.: 2011, Relating white light and *in situ* observations of coronal mass ejections: a review. *J. Atmos. Solar-Terr. Phys.* **73**, 1201 – 1213. doi:10.1016/j.jastp.2010.08.015.

Rouillard, A.P., Lavraud, B., Sheeley, N.R., Davies, J.A., Burlaga, L.F., Savani, N.P., Jacquey, C., Forsyth, R.J.: 2010, White light and *in situ* comparison of a forming merged interaction region. *Astrophys. J.* **719**, 1385 – 1392. doi:10.1088/0004-637X/719/2/1385.

Russell, C.T., Mulligan, T.: 2002, On the magnetosheath thicknesses of interplanetary coronal mass ejections. *Planet. Space Sci.* **50**, 527 – 534. doi:10.1016/S0032-0633(02)00031-4.

Schwenn, R., dal Lago, A., Huttunen, E., Gonzalez, W.D.: 2005, The association of coronal mass ejections with their effects near the Earth. *Ann. Geophys.* **23**, 1033 – 1059.

Sheeley, N.R. Jr., Wang, Y.-M., Hawley, S.H., Brueckner, G.E., Dere, K.P., Howard, R.A., Koomen, M.J., Korendyke, C.M., Michels, D.J., Paswaters, S.E., Socker, D.G., St. Cyr, O.C., Wang, D., Lamy, P.L., Llebaria, A., Schwenn, R., Simnett, G.M., Plunkett, S., Biesecker, D.A.: 1997, Measurements of flow speeds in the corona between 2 and 30 R_{Sun}. *Astrophys. J.* **484**, 472 – 478. doi:10.1086/304338.

Smith, Z.K., Dryer, M., McKenna-Lawlor, S.M.P., Fry, C.D., Deehr, C.S., Sun, W.: 2009, Operational validation of HAFv2's predictions of interplanetary shock arrivals at Earth: declining phase of Solar Cycle 23. *J. Geophys. Res.* **114**, A05106. doi:10.1029/2008JA013836.

Taktakishvili, A., Kuznetsova, M., MacNeice, P., Hesse, M., Rastätter, L., Pulkkinen, A., Chulaki, A., Odstrcil, D.: 2009, Validation of the coronal mass ejection predictions at the Earth orbit estimated by ENLIL heliosphere cone model. *Space Weather* **7**, S03004. doi:10.1029/2008SW000448.

Tappin, S.J.: 2006, The deceleration of an interplanetary transient from the Sun to 5 AU. *Solar Phys.* **233**, 233 – 248. doi:10.1007/s11207-006-2065-2.

Temmer, M., Vršnak, B., Veronig, A.M.: 2007, Periodic appearance of coronal holes and the related variation of solar wind parameters. *Solar Phys.* **241**, 371 – 383. doi:10.1007/s11207-007-0336-1.

Temmer, M., Rollett, T., Möstl, C., Veronig, A.M., Vršnak, B., Odstrčil, D.: 2011, Influence of the ambient solar wind flow on the propagation behavior of interplanetary coronal mass ejections. *Astrophys. J.* **743**, 101 – 112. doi:10.1088/0004-637X/743/2/101.

Temmer, M., Vršnak, B., Rollett, T., Bein, B., de Koning, C.A., Liu, Y., Bosman, E., Davies, J.A., Möstl, C., Žic, T., Veronig, A.M., Bothmer, V., Harrison, R., Nitta, N., Bisi, M., Flor, O., Eastwood, J., Odstrcil, D., Forsyth, R.: 2012, Characteristics of kinematics of a coronal mass ejection during the 2010 August 1 CME–CME interaction event. *Astrophys. J.* **749**, 57. doi:10.1088/0004-637X/749/1/57.

Vršnak, B.: 2001a, Deceleration of coronal mass ejections. *Solar Phys.* **202**, 173 – 189.

Vršnak, B.: 2001b, Dynamics of solar coronal eruptions. *J. Geophys. Res.* **106**, 25249 – 25260. doi:10.1029/2000JA004007.

Vršnak, B., Gopalswamy, N.: 2002, Influence of the aerodynamic drag on the motion of interplanetary ejecta. *J. Geophys. Res.* **107**, SSH2. doi:10.1029/2001JA000120.

Vršnak, B., Žic, T.: 2007, Transit times of interplanetary coronal mass ejections and the solar wind speed. *Astron. Astrophys.* **472**, 937 – 943. doi:10.1051/0004-6361:20077499.

Vršnak, B., Temmer, M., Veronig, A.M.: 2007, Coronal holes and solar wind high-speed streams: I. Forecasting the solar wind parameters. *Solar Phys.* **240**, 315 – 330. doi:10.1007/s11207-007-0285-8.

Vršnak, B., Vrbanec, D., Čalogović, J.: 2008, Dynamics of coronal mass ejections. The mass-scaling of the aerodynamic drag. *Astron. Astrophys.* **490**, 811 – 815. doi:10.1051/0004-6361:200810215.

Vršnak, B., Ruždjak, D., Sudar, D., Gopalswamy, N.: 2004, Kinematics of coronal mass ejections between 2 and 30 solar radii. What can be learned about forces governing the eruption? *Astron. Astrophys.* **423**, 717 – 728. doi:10.1051/0004-6361:20047169.

Vršnak, B., Sudar, D., Ruždjak, D., Žic, T.: 2007, Projection effects in coronal mass ejections. *Astron. Astrophys.* **469**, 339 – 346. doi:10.1051/0004-6361:20077175.

Vršnak, B., Žic, T., Falkenberg, T.V., Möstl, C., Vennerstrom, S., Vrbanec, D.: 2010, The role of aerodynamic drag in propagation of interplanetary coronal mass ejections. *Astron. Astrophys.* **512**, A43. doi:10.1051/0004-6361/200913482.

Webb, D.F., Howard, T.A., Fry, C.D., Kuchar, T.A., Odstrcil, D., Jackson, B.V., Bisi, M.M., Harrison, R.A., Morrill, J.S., Howard, R.A., Johnston, J.C.: 2009, Study of CME propagation in the inner heliosphere: SOHO LASCO, SMEI and STEREO HI observations of the January 2007 events. *Solar Phys.* **256**, 239 – 267. doi:10.1007/s11207-009-9351-8.

Wood, B.E., Howard, R.A., Socker, D.G.: 2010, Reconstructing the morphology of an evolving coronal mass ejection. *Astrophys. J.* **715**, 1524 – 1532. doi:10.1088/0004-637X/715/2/1524.

Xie, H., Ofman, L., Lawrence, G.: 2004, Cone model for halo CMEs: application to space weather forecasting. *J. Geophys. Res.* **109**, A03109. doi:10.1029/2003JA010226.

Yashiro, S., Gopalswamy, N., Michalek, G., St. Cyr, O.C., Plunkett, S.P., Rich, N.B., Howard, R.A.: 2004, A catalog of white light coronal mass ejections observed by the SOHO spacecraft. *J. Geophys. Res.* **109**, A07105. doi:10.1029/2003JA010282.

Zhang, J., Dere, K.P., Howard, R.A., Bothmer, V.: 2003, Identification of solar sources of major geomagnetic storms between 1996 and 2000. *Astrophys. J.* **582**, 520 – 533. doi:10.1086/344611.

Zhao, X.P., Plunkett, S.P., Liu, W.: 2002, Determination of geometrical and kinematical properties of halo coronal mass ejections using the cone model. *J. Geophys. Res.* **107**, SSH13. doi:10.1029/2001JA009143.